Biology Direct

RESEARCH

Open Access

hsa_circ_0020093 suppresses ovarian cancer progression by modulating LRPPRC activity and miR-107/LATS2 signaling

Yu Sun[1,2], Xiyi Chen[1], Yaqian Shi[1], Fang Teng[1], Chencheng Dai[1], Lili Ge[1*], Juan Xu[1*] and Xuemei Jia[1*]

Abstract

A substantive body of evidence has demonstrated the significant roles of circular RNA (circRNA) in cancer. However, the contribution of dysregulated circRNAs to ovarian cancer (OC) remains elusive. We aim to elucidate the critical roles and mechanisms of hsa_circ_0020093, which was demonstrated to be downregulated in OC tissues in our previous study. In this study, we confirmed the decreased expression of hsa_circ_0020093 in OC tissues and cell lines and demonstrated the negative correlation between its expression and FIGO stage, abdominal implantation and CA125 level of OC patients. Through gain and loss of function studies, we confirmed the inhibitory role of hsa_circ_0020093 in ovarian tumor growth in vitro and in vivo. Mechanistically, based on the peri-nuclear accumulation of hsa_circ_0020093, we discovered the interaction between hsa_circ_0020093 and the mitochondrial protein LRPPRC by RNA pull-down, mass spectrometry, RNA Binding Protein Immunoprecipitation. As a result, qRT-PCR and transmission electron microscopy results showed that the mitochondria mRNA expression and mitochondria abundance were decreased upon hsa_circ_0020093-overexpression. Meanwhile, we also unearthed the hsa_circ_0020093/miR-107/LATS2 axis in OC according to RNA-sequencing, RIP and luciferase reporter assay data. Furthermore, LRPPRC and LATS2 are both reported as the upstream regulators of YAP, our study also studied the crosstalk between hsa_circ_0020093, LRPPRC and miR-107/LATS2, and unearthed the up-regulation of phosphorylated YAP in hsa_circ_0020093-overexpressing OC cells and xenograft tumors. Collectively, our study indicated the novel mechanism of hsa_circ_0020093 in suppressing OC progression through both hsa_circ_0020093/LRPPRC and hsa_circ_0020093/miR-107/LATS2 axes, providing a potential therapeutic target for OC patients.

Keywords Ovarian cancer, hsa_circ_0020093, miR-107, LAST2, LRPPRC

Introduction

Ovarian cancer (OC) is the second most common cause of gynaecologic cancer death worldwide [1]. Although many cancer patients benefit from the development of technology in early detection, surgery and drugs, OC patients still suffer from relapse (70–90%) and stand with lifelong cancer care. Compared with the five-year survival rate of cervical cancer (66.3%) and breast cancer (90.3%), the five-year survival rate of OC is only 49% [2].

Although the early-stage disease is highly curable, most women diagnosed with stage III/IV disease, and over 75% of patients with late-stage OC die of their disease [2].

*Correspondence:
Lili Ge
gll7906gll@njmu.edu.cn
Juan Xu
xujuannj@njmu.edu.cn
Xuemei Jia
xmjia@njmu.edu.cn
[1] Department of Gynecology, Women's Hospital of Nanjing Medical University (Nanjing Women and Children's Healthcare Hospital), 123 Tianfei Xiang, Mochou Road, Nanjing 210004, China
[2] School of Pharmacy, Queen's University Belfast, Medical Biology Centre, 97 Lisburn Road, Belfast BT9 7BL, UK

Some people believe that improving screening options for OC could be helpful. However, the UK Collaborative Trial of Ovarian Cancer Screening reported that screening did not significantly reduce ovarian and tubal cancer mortality and the reduced incidence of stage III or IV disease was insufficient to save lives [3]. Accordingly, it is important to identify the mechanism of OC progression to seek a precise therapeutic target to enhance the survival rate.

Over the past decade, circular RNAs (circRNAs) have been discovered as a large class of non-coding RNA molecules [4]. Numerous individual circRNAs present different abundance in tumors versus adjacent non-cancer tissues and are significantly associated with clinical characteristics such as FIGO stage, histological grade and metastasis [5]. Also, plenty of studies report that their dysregulation contributed to cancer development via diverse mechanisms like miRNA sponging, protein interactors or translation templates [5]. Based on their well-established functional roles in tumorigenesis, circRNAs have shown great prospects in precision cancer therapy [6, 7].

In addition, circRNAs, particularly those with tumor-suppressive properties, could sponge and inactivate "deleterious miRNAs and/or proteins" and simultaneously enhance the expression of "beneficial proteins" within pathophysiological contexts. This miRNA and protein sponge mechanism underscores the potential of circRNAs to act as therapeutic agents. Consequently, investigating these tumor-suppressive circRNAs and their underlying mechanisms could yield valuable insights for the development of circRNA-based drugs.

Our previous studies identified five downregulated circRNAs in OC compared to normal ovarian tissues [8], suggesting their potential role in suppressing the progression of the disease. Among these, hsa_circ_0020093, also named as circATRNL1, showed the most significant reduction, leading us to prioritize it for further investigation. During the study, it was reported that hsa_circ_0020093 inhibited angiogenesis and metastasis in OC through sponging miR-378 [9]. Lyu et al. proved that hsa_circ_ 0020093 had protein translation potential [10]. In this study, we unveil a novel mechanism of hsa_circ_0020093 through sponging both LRPPRC and miR-107 to modulate OC progression. These findings provide new insights and suggest that hsa_circ_0020093 could be a promising biomarker and therapeutic target for OC.

Materials and methods

Reagents and cell culture

The information for the source and working dilution of antibodies are provided in Online Resource 1, Supplementary Table 1. The information of reagents, kits and cell culture media is provided in Online Resource 1, Supplementary Table 2.

A2780, OVCAR3, and CAOV3 cells were purchased from Shanghai Mingjing Biology Co., Ltd. (Shanghai, China); SKOV3 and 293T cells were purchased from the National Collection of Authenticated Cell Cultures (Shanghai, China); The immortalized ovarian surface epithelial cell line IOSE386 cell was a gift from Dr Zhu Jin, Huadong Medical Institute of Biotechniques (Nanjing, China). All cell lines have been authenticated by STR profiling and tested for mycoplasma contamination negative. All the cell lines were routinely cultured in DMEM (A2780, IOSE386, CAOV3), McCoy's 5A (SKOV3), and RPMI-1640 (OVCAR3, 293 T). All the culture media was purchased from Jiangsu KeyGEN BioTECH Co., Ltd. (Nanjing, China). Media was supplemented with 10–20% FBS and 1% Pen/Strep.

Clinical samples

Forty-four OC tissues and seventeen adjacent cancer tissues for RNA extraction were collected from the Women's Hospital of Nanjing Medical University (Nanjing Women and Children's Healthcare Hospital) between Oct. 2018 and Dec. 2021. A total of 44 EOC paraffin sections from the pathology department were obtained from Jan. 2015 to Dec. 2019. The final diagnosis of each tissue was confirmed by histopathology, and the tumor stage was classified according to FIGO classification. All the patients signed the informed consent forms and our study methodologies conformed to the Declaration of Helsinki. The Ethical Committee of Women's Hospital of Nanjing Medical University approved this study.

Plasmids, small interfering RNA, miRNA and transfection

Hsa_circ_0020093 cDNA was synthesized and cloned into the vector pLC5-ciR (named OE-circ) purchased from Geneseed Biotech Co., Ltd. (Guangzhou, China) and an empty pLC5-ciR (named Control) was served as control. LRPPRC cDNA was synthesized and cloned into the vector pcDNA3.1 purchased from GENEbay Co., Ltd (Nanjing, China). The small interfering RNA and miRNA mimics were purchased from Ribobio Biotech Co., Ltd. (Guangzhou, China). Their sequences were in Online Resource 1, Supplementary Table 3 and a scramble siRNA or miRNA was synthesized as control.

Transfection was performed using Lipofectamine 3000 (Invitrogen, Waltham, MA, USA) following the manufacturer's instructions. Total proteins and RNA were collected 48 h post-transfection. Functional experiments were performed 24 h post-transfection.

Generation of stable hsa_circ_0020093 and LRPPRC overexpression cell lines

Hsa_circ_0020093-overexpressing and control lentivirus were purchased from Geneseed Biotech Co. Lentivirus with LRPPRC-Myc-tag fusion and control lentivirus were purchased from GENEbay Co., Ltd. SKOV3 (2×10^5) and OVCAR3 (2.5×10^5) cells were seeded in six-well plates infected with lentivirus at a multiplicity of infection (MOI) of 2, selected with puromycin (2 μg/ml) for 1 week and expanded. Overexpression efficiency was assessed by RT-qPCR and western blotting.

Cell proliferation, migration and invasion assay

The proliferation of SKOV3 and OVCAR3 cells were analyzed using the cell counting kit-8 (CCK-8) as previously described with moderate changes [8]. At 24 h post-transfection, 2×10^3 cells were seeded in each well of 96-well plates. The absorbance at 450 nm was measured by BioTek Synergy H4 instrument (BioTek Instruments, Winooski, VT, USA) once every day for the following 3 days. The migration and invasion were measured using Transwell assay with or without Matrigel as in our previous study [8]. The migrated and invaded cells were stained with crystal violet and then dissolved by protein lysis buffer. The OD density of lysis at 562 nm showed the quantification of migration and invasion.

Flow cytometry

Flow cytometry was performed to analyze cell apoptosis. After being transfected with hsa_circ_0020093 or pLC5-ciR control plasmids and incubated for 24 h, cells were pretreated with cisplatin (10 μg/mL) for another 24 h. Then they were harvested and double stained with Annexin V-APC and PI. The results were analyzed by flow cytometer (Beckman Coulter).

Tumor formation assay in vivo

The animal experiment was approved by the Ethics Committee of Experimental Animal Welfare of Nanjing Medical University. Twelve 6-week-old BALB/c female nude mice were randomly divided into two groups. After adaptive feeding for three days, 1×10^7 stable overexpressed hsa_circ_0020093 SKOV3 cells and control SKOV3 cells were suspended in 100 μL PBS and subcutaneously injected into the right armpit of each BALB/c nude mouse, respectively. The health condition of the mice was observed daily and the volume of the tumors was calculated every two or three days using the following formula: volume (mm^3) = length (mm) × width^2 (mm^2)/2. The animals were sacrificed 18 days after injection, and the tumors were isolated, photographed and weighed. Hematoxylin–eosin staining was used to verify tumor characteristics.

RNA extraction and quantitative real-time PCR (RT-qPCR)

Tissue samples and cells' total RNA were extracted using GeneJET RNA Purification Kit (Thermo), and synthesized into cDNA using HiScript III RT SuperMix for qPCR kit (Vazyme, Nanjing, China). Then qPCR was employed using SYBR Green (Thermo). The nuclear and cytoplasmic cell fraction was isolated using the PARIS™ kit (Thermo) following the manufacturer's instructions. Relative RNA expression was calculated using the $2^{-\triangle\triangle CT}$ method while hsa_circ_0020093 expression in tissues was calculated using $2^{-\triangle CT}$. *ACTB*, *GAPDH*, *18S*, and *U6* were the internal controls. *U6* was also the internal control of miRNA expression and *18S* was the internal control of MT-mRNA expression. The primer sequences are shown in Online Resource 1, Supplementary Table 4.

Immunoblotting

Cells were lysed by Radioimmunoprecipitation assay (RIPA) buffer (Servicebio, Wuhan, China) supplemented with protease inhibitors (Thermo) as well as phosphatase inhibitors (Servicebio). Briefly, equal amounts of protein were resolved in 8%, 10% or 12% SDS-PAGE gel and transferred to the PVDF membrane. Membranes were blocked in 5% non-fat milk in TBST (TBS with 0.1% tween-20) for 2 h at room temperature, then incubated with primary antibodies at 4 °C overnight and secondary antibodies at room temperature for 1 h. β-actin and GAPDH were used to verify equal loading. Image J (image processing and analysis in JAVA, NIH) was applied to quantify the protein level relative to loading control.

For immunoblotting analysis of caspase 3 and cleaved caspase-3, cells were pretreated with cisplatin (10 μg/mL) for 24 h before protein extraction.

RNA immunoprecipitation (RIP)

RNA immunoprecipitation was performed using Magna RIP RNA-Binding Protein Immunoprecipitation Kit (Millipore, Burlington, MA, USA), following the manufacturer's instructions. Briefly, 2×10^7 cells were collected by RIP lysis buffer. Anti-AGO2, anti-LRPPRC and anti-IgG were first bound to magnetic beads for 30 min at room temperature. Next, cell lysates were incubated with beads-antibody complex overnight at 4 °C. Then, the RNAs binding to specific proteins were eluted, reverse transcripted to cDNA and quantified by RT-qPCR.

RNA sequencing

Total RNA from stable hsa_circ_0020093-overexpressed SKOV3 cells and control SKOV3 cells were extracted for RNA sequencing by Shanghai Biotechnology Corporation (China). Briefly, RNA quality and quantity

were assessed by Bioanalyzer 2100 (Agilent Technologies, USA) and NanoDrop 2000 spectrophotometer (Thermo), respectively. Samples with RNA Integrity Number (RIN) ≥ 7 were applied for RNA-seq transcriptome library construction by VAHTS Universal V6 RNA-seq Library Prep Kit for Illumina® (Vazyme, China) according to the manufacturer's instruction. Quantified and qualified libraries were sequenced on the Illumina NovaSeq 6000 sequencing platform. TargetScan, miRTarBase (https://mirtarbase.cuhk.edu.cn/) and miRDB (http://mirdb.org/) were employed to predict mRNAs possibly targeted by miR-107.

Luciferase reporter assay

Linear sequences of wild-type and hsa-miR-181a-5p or hsa-miR-107 binding sites mutant type of hsa_circ_0020093 were cloned into the luciferase reporter vector pmirGLO, respectively. 293T cells were co-transfected with wild- or mutant-type of reporter plasmids and miRNA mimics. Then the relative luciferase activity was determined by using Promega Dual-Luciferase Reporter Assay. The renilla luciferase activity was used as an internal control.

RNA Fluorescence in situ hybridization (FISH) and Immunofluorescence (IF)

FISH and immunofluorescence staining were performed to detect hsa_circ_0020093 subcellular localization. FISH assays were conducted in accordance with the protocols outlined in the previous publication [11]. Cells were first fixed with 4% polyoxymethylene for 10 min at room temperature and permeabilized with 0.5% Triton X-100 for 5 min at 4 °C, then blocked with 1% BSA and 22.52 mg/mL glycine in PBST (PBS + 0.1%Tween 20) for 30 min at room temperature. Cells were incubated with primary antibody overnight at 4 °C and Alexa Fluor labeled-488 or labeled-647 for 1 h at room temperature. After being washed with PBST 3 times, cells were stained with Cy3 labeled probes targeting the hsa_circ_0020093 junction region for 10 h at 37 °C. Then cells were washed separately with 4 × saline-sodium citrate buffer (SSC), 2 × SSC and 1 × SSC. Nucleus was dyed with DAPI and observed by confocal microscopy (Leica, German).

Immunohistochemistry (IHC)

Paraffin slides were stained with antibodies using the IHC kit (Proteintech, USA) as previously described [12]. IHC scores were calculated by Image J, and the formula = High positive cell amounts × 3 + Medium positive cell amounts × 2 + Low Positive cell amounts × 1 + Negative cell amounts × 0 [13].

RNA pull-down, silver stain and mass spectrometry assay

RNA pull-down assay was performed following the instructions of Pierce Magnetic RNA–Protein Pull-Down Kit (Thermo, USA) with moderate adjustments according to previous reports [14]. Two biotin-labeled DNA probes, complemented with hsa_circ_0020093 junction site, were synthesized by Ribobio and well mixed. The sequences were provided in Online Resource 1, Supplementary Table 4. Total RNA was extracted and incubated with 100 pmol mixed probes at 70 °C for 5 min. Then RNA was slowly cooled down (1.5 °C/min) to room temperature. Hsa_circ_0020093-probes mix was co-rotated with streptavidin magnetic beads in RNA capture buffer for 30 min at room temperature. Notably, before incubating lysates with beads, the specificity of probes binding hsa_circ_0020003 was verified by RT-qPCR. In the meantime, a master mix for RNA–Protein binding reaction was prepared, containing 10 μL 1 × Protein-RNA Binding Buffer, 30 μL 50% glycerol, 30 μL cell lysate from SKOV3 or OVCAR3 cells and 30 μL nuclease-free water. After rotation, the master mix was incubated with the beads overnight at 4 °C. The RNA-binding proteins were eluted by elution buffer at 37 °C for 30 min with vibration.

The proteins binding with control probes and circ probes were separated by SDS-PAGE and stained with silver dye. The distinguished stripes were cut and analyzed by mass spectrometry. The peptides were identified by Mascot software, and the Mascot value ≤ 0.05 was the filtering criteria. Then the identified proteins were ranked by Q-score and abundance.

Bioinformatic online platforms or tools

Three algorithms including RegRNA (http://RegRNA.mbc.NCTU.edu.tw/), TargetScan (https://www.targetscan.org/vert_71/) and Starbase (https://starbase.sysu.edu.cn/) were used to predict potential miRNAs sponged by hsa_circ_0020093. The miRNA microarray dataset GSE47841 was applied to analyze differentially expressed miRNAs between OC tissues and normal ovary tissues using dbDEMC database (https://www.biosino.org/dbDEMC/index). The fold change > 1.5 or < 0.667 with adjusted $P < 0.05$ was set as the threshold. The potential target mRNAs of individual miRNAs were predicted by TargetScan, miRTarbase (http://mirtarbase.mbc.nctu.edu.tw/php/index.php) and miRDB (https://mirdb.org/). GEPIA database (http://gepia.cancer-pku.cn/) was used to identify differentially expressed mRNAs between OC tissues and normal ones.

Apart from several tools to predict and analyze circRNA-miRNA-mRNA network and miRNA abundance mentioned above, the Cancer Proteogenomic Data Analysis Site (cProSite), an online-applicable interactive

platform providing data visualization of the National Cancer Institute's Clinical Proteomic Tumor Analysis Consortium (CPTAC) and National Cancer Institute's International Cancer Proteogenome Consortium (ICPC) datasets, has been used in this article to illustrate LRPPRC protein abundance between ovarian cancer and normal adjacent tissues [15].

Statistical analysis

All experiments were carried out at least three times and data from one representative experiment are shown. Data from three independent experiments are expressed as mean ± standard deviation (SD). For comparison between two groups, student's t test (unpaired) was applied for data with normal distribution while others used the Mann–Whitney U test. When more than two groups were compared, one-way ANOVA was performed followed by Tukey's test. A two-way ANOVA with the independent factors of time and grouping was used in CCK-8 assay and tumor volume growth analysis for each dependent variable. The relationship between hsa_circ_0020093 expression, LRPPRC protein level and various clinicopathological variables were analyzed by chi-square tests. Overall survival and recurrence-free survival were determined using the Kaplan–Meier method, and the significance of the differences between the survival rates was calculated by the log-rank test. The diagnostic efficacy of has_circ_0020093 in clinical specimens was evaluated using the receiver operating characteristic (ROC) curve analysis. The area under the curve (AUC) was calculated to evaluate the diagnostic performance. The evaluation was conducted using "ROC curve" analysis within the "Column analyses" module in GraphPad Prism 9.0. P value < 0.05 was defined as statistically significant. Statistical analyses were performed using SPSS software 26.0 or GraphPad Prism 9.0.

Results

hsa_circ_0020093 inhibits OC progression in vitro and in vivo

Our previous study first identified the circRNA, hsa_circ_0020093, back-spliced from 4 exons (exon 2 to exon5, spliced length: 536 bp) of attractin-like protein 1 (*ATRNL1*) mRNA, also named as circATRNL1, and demonstrated that hsa_circ_0020093 was downregulated in ovarian cancer (OC) tissues compared with normal ovarian tissues [8]. In this study, its low expression in OC tissues (n = 44) was verified compared with adjacent normal tissues (n = 17) (Fig. 1A) and in OC cell lines (CAOV3, OVAR3, A2780, SKOV3) as compared with normal ovarian epithelial cells IOSE386 (Fig. 1B). Then we investigated the expression of hsa_circ_0020093 and the clinicopathological characteristics of OC patients, the results showed that hsa_circ_0020093 had good diagnostic utility in OC tissues (Fig. 1C), and its expression was negatively correlated with FIGO stages, grades, peritoneal implantation, and CA125 levels (Table 1), indicating that hsa_circ_0020093 might participate in OC progression.

Then we aim to unearth the potential function and mechanism of hsa_circ_0020093. The forced expression and silencing of hsa_circ_0020093 were verified by RT-qPCR after transfection of OE-circ vector, small interfering RNA (siRNA) targeting hsa_circ_0020093, control vector and siNC, respectively, whereas *ATRNL1* mRNA expression was unaffected (Online Resource 2, Supplementary Fig. 1). Knockdown of hsa_circ_0020093 increased cell viability of SKOV3 and OVCAR3 cells in CCK8 assays (Fig. 1D). Transwell assays with or without matrigel revealed that silencing hsa_circ_0020093 promoted the migratory and invasive ability of SKOV3 and OVCAR3 cells (Fig. 1E–F). Besides, a decrease in apoptosis induced by cisplatin, as indicated by the western blot analysis of cleaved caspase-3, was observed in SKOV3 and OVCAR3 cells following the silencing hsa_circ_0020093 (Fig. 1G). In contrast, the overexpression of hsa_circ_0020093 inhibited cell proliferation, migration and invasion while promoting apoptosis in SKOV3 and OVCAR3 cells (Fig. 2A–F).

After identifying the role of hsa_circ_0020093 in vitro, we constructed a hsa_circ_0020093 stably overexpressed SKOV3 cell line by infecting with hsa_circ_0020093-overexpressed lentivirus and confirmed the overexpression efficiency of hsa_circ_0020093, in which the mRNA expression of *ATRNL1* was nearly unchanged as compared with the control group (Fig. 2G). Then we investigated the in vivo role of hsa_circ_0020093 on tumor growth by subcutaneously injecting the hsa_circ_0020093-overexpressing and control SKOV3 cells into the female Balb/c nude mice. As shown in Fig. 2H–I, the tumor volume was significantly smaller in mice injected with hsa_circ_0020093-overexpressing SKOV3 cells than in mice injected with control SKOV3 cells. And the tumor weight was considerably lighter in the hsa_circ_0020093-overexpressing group (Fig. 2J). Moreover, we witnessed a less positive rate of Ki67 in the hsa_circ_0020093-overexpressing group (Fig. 2K–L). Based on the above, hsa_circ_0020093 suppressed OC cell proliferation, migration and invasion while promoting OC cell apoptosis in vitro and inhibited tumor growth in vivo.

hsa_circ_0020093 interacts with LRPPRC, a pro-oncogenic protein in OC progression

The potential mechanisms of circRNAs are closely related to their subcellular localization [16]. Thus, we examined the subcellular localization of hsa_circ_0020093

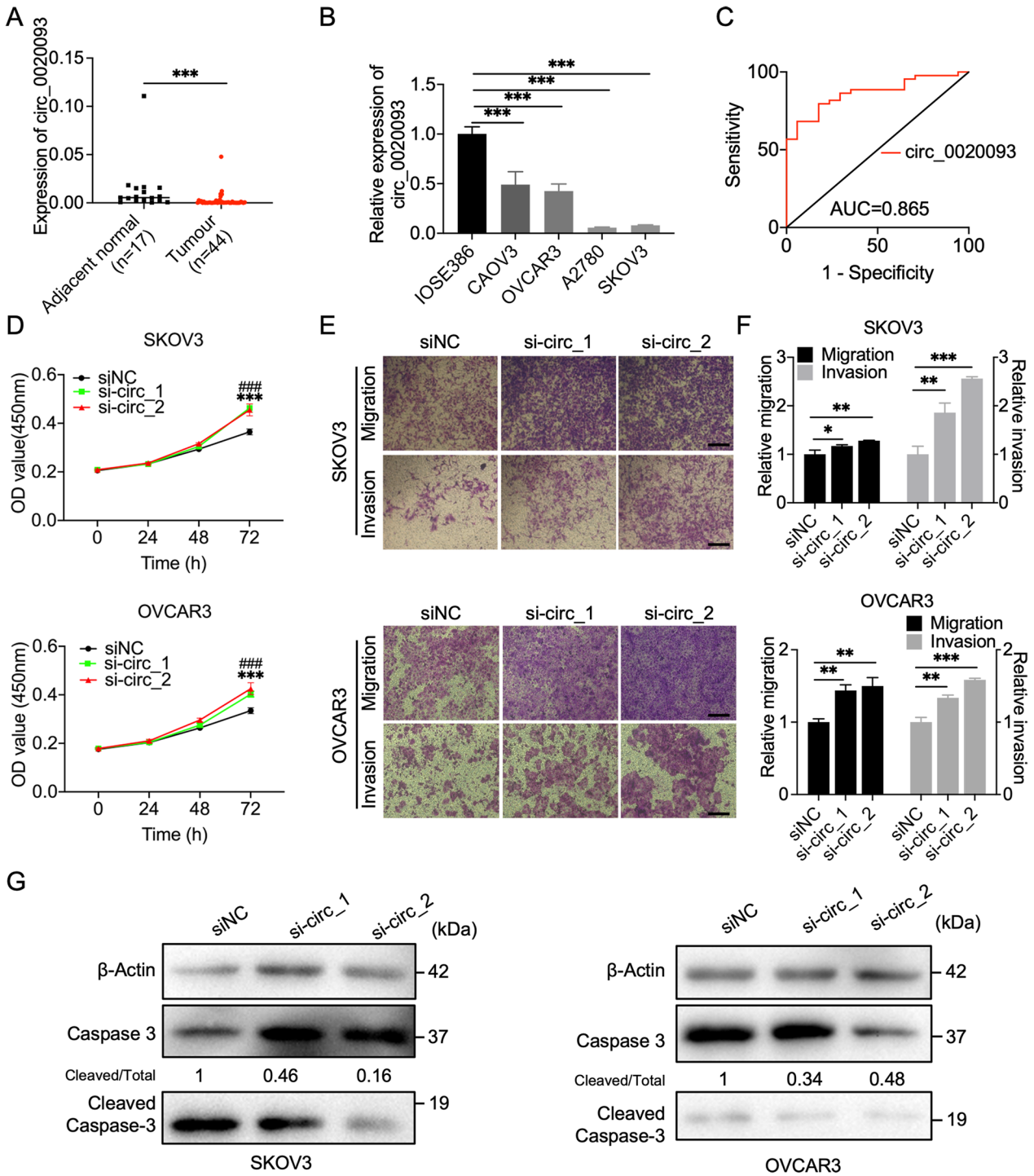

Fig. 1 Silencing of hsa_circ_0020093 enhances the malignant behavior of OC cells in vitro. **A** RT-qPCR analysis of hsa_circ_0020093 (abbreviated as circ_0020093 in the figures) expression in OC tissues (n = 44) and adjacent normal tissues (n = 17). *P* value was calculated by Mann–Whitney U test. **B** RT-qPCR analysis of hsa_circ_0020093 expression in IOSE386, CAOV3, OVCAR3, A2780 and SKOV3 cells. The expression of hsa_circ_0020093 in IOSE386 served as control. *P* value was calculated by two-tailed Student's t-test. **C** ROC analysis of hsa_circ_0020093 expression in OC and adjacent normal tissues. AUC: Area under the curve. **D** The effect of hsa_circ_0020093-silencing on SKOV3 and OVCAR3 cell viability was determined by CCK8 assay. "*" represents statistical significance between siNC and si-circ_1 group, while "#" represents statistical significance between siNC and si-circ_2 group. *P* value was calculated by two-way ANOVA. **E–F** The effects of hsa_circ_0020093 silencing on cell migration and invasion ability of SKOV3 and OVCAR3 cells were assessed by transwell with or without matrigel assay. Scale bar: 200 μm. *P* value was calculated by two-tailed Student's t-test. **G** Western blot analysis of caspase-3 and cleaved caspase-3 expression after silencing hsa_circ_0020093 in SKOV3 and OVCAR3 cells. The activity of caspase-3 was calculated by cleaved caspase-3/total caspase-3. ns, not significant; $^{*}P < 0.05$; $^{**}P < 0.01$; $^{***}P < 0.001$

Table 1 Correlation between hsa_circ_0020093 expression and clinicopathologic factors of OC patients

Parameter		hsa_circ_0020093 (High, n = 22)	hsa_circ_0020093 (Low, n = 22)	*P* value
Age	≤ 50	10	7	0.353
	> 50	12	15	
FIGO stage	I + II	14	7	**0.035***
	III + IV	8	15	
Grade	Low	10	1	**0.002****
	High	12	21	
Lymphatic metastasis	No	15	11	0.222
	Yes	7	11	
Peritoneal implantation	No	12	4	**0.012***
	Yes	10	18	
CA125 (U/mL)	< 35	7	0	**0.004****
	≥ 35	15	22	

The bold numbers refer to the P value statistically significant, ** indicates that $P < 0.01$

via RT-qPCR of the nuclear and cytoplasmic fraction of RNA and RNA fluorescence in situ hybridization (FISH). Figure 3A–B show that hsa_circ_0020093 existed in both the nucleus and cytoplasm of SKOV3 and OVCAR3 cells. Interestingly, it was mainly enriched in the perinuclear region in cytoplasm, similar with mitochondria localization in the cytoplasm.

The localization of hsa_circ_0020093 in nuclear and peri-nuclear region of the cytoplasm indicates that it may bind with the specific proteins that showed the same localization. Biotin-labelled DNA probes specific for hsa_circ_0020093 were constructed and then used in the RNA pull-down assay to discover hsa_circ_0020093 binding proteins. First, the probes' efficiency and specificity of capturing hsa_circ_0020093 were confirmed (Online Resource 2, Supplementary Fig. 2A). The specified hsa_circ_0020093 binding proteins were separated and revealed by SDS-PAGE and silver staining (Fig. 3C). The different bands were sent for mass spectrometric analysis, and 19 proteins specifically enriched in circ probes' nor in control probes' groups were identified. Among these 19 proteins, LRPPRC ranked top in abundance and Q-score (Fig. 3D), and UniProt (https://www.uniprot.org/uniprotkb/P42704/entry#subcellular_location) indicated its localization within mitochondria and the nucleus, which was overlapped with hsa_circ_0020093's subcellular localization. Western blot following the RNA pull-down assay confirmed that hsa_circ_0020093 could interact with LRPPRC (Fig. 3E). LRPPRC RIP assay showed the enrichment of hsa_circ_0020093 in LRPPRC binding RNAs compared with the control IgG (Fig. 3F). The FISH combining IF assay demonstrated the co-localization of LRPPRC and hsa_circ_0020093 in mitochondria, as indicated by TOM20, a mitochondrial import receptor subunit localized in the outer membrane of mitochondria (Fig. 3G). These results proved that hsa_circ_0020093 and LRPPRC interacted with each other in mitochondria.

LRPPRC is a multifunctional protein which regulates energy metabolism and maturation and translocation of certain mRNAs [17]. Its high expression indicated poor prognosis in various cancers like prostate cancer [18], pancreatic cancer [19] and gastric cancer [20]. We noticed that LRPPRC was also highly expressed in OC tissues compared with adjacent normal tissues in CPTAC and ICPC database using cProSite analysis platform (Fig. 3H). Moreover, the protein level of LRPPRC was positively correlated with FIGO stage, peritoneal implantation, and negatively correlated with overall survival and recurrence-free survival of EOC patients (n = 22 in each group) (Fig. 3I–J, Online Resource 2, Supplementary Fig. 2B and Table 2). Meanwhile, silencing of *LRPPRC* impaired proliferation and promoted apoptosis of SKOV3 and OVCAR3 cells (Online Resource 2, Supplementary Fig. 2C–E). These

(See figure on next page.)

Fig. 2 Overexpression of hsa_circ_0020093 represses OC progression in vitro and in vivo. **A** The effect of hsa_circ_0020093 overexpression on SKOV3 and OVCAR3 cell viability was determined by CCK8 assay. *P* value was calculated by two-way ANOVA. **B–C** The effects of hsa_circ_0020093 overexpression on cell migration and invasion ability of SKOV3 and OVCAR3 cells were assessed by transwell assays with or without matrigel. Scale bar: 200 μm. *P* value was calculated by two-tailed Student's t-test. **D–E** Flow cytometry was used to detect cell apoptosis, APC(+)/PI(−) indicates early apoptosis while APC(+)/PI(+) indicates late apoptosis. **F** Western blot analysis of caspase-3 and cleaved caspase-3 expression after overexpression of hsa_circ_0020093 in SKOV3 and OVCAR3 cells. The activity of caspase-3 was calculated by cleaved caspase-3/total caspase-3. **G** RT-qPCR analysis of the RNA level of hsa_circ_0020093 and *ATRNL1* mRNA in SKOV3 cells stably overexpressing hsa_circ_0020093 and control. *P* value was calculated by two-tailed Student's t-test. **H** Xenograft tumors of hsa_circ_0020093-overexpressing and control SKOV3 cells (n = 6). **I** The xenograft tumor growth of hsa_circ_0020093-overexpressing and control SKOV3 cells. *P* value was calculated by two-way ANOVA. **J** The xenograft tumor weight of hsa_circ_0020093-overexpressing and control SKOV3 cells. *P* value was calculated by two-tailed Student's t-test. **K** The representative images of tumor tissues stained with Ki67 (Left). **L** Ki67-positive degree in tumor tissues was calculated by immunohistochemistry (IHC) scores. Scale bar: 100 μm. *P* value was calculated by two-tailed Student's t test. ns, not significant; $^{*}P < 0.05$; $^{**}P < 0.01$; $^{***}P < 0.001$

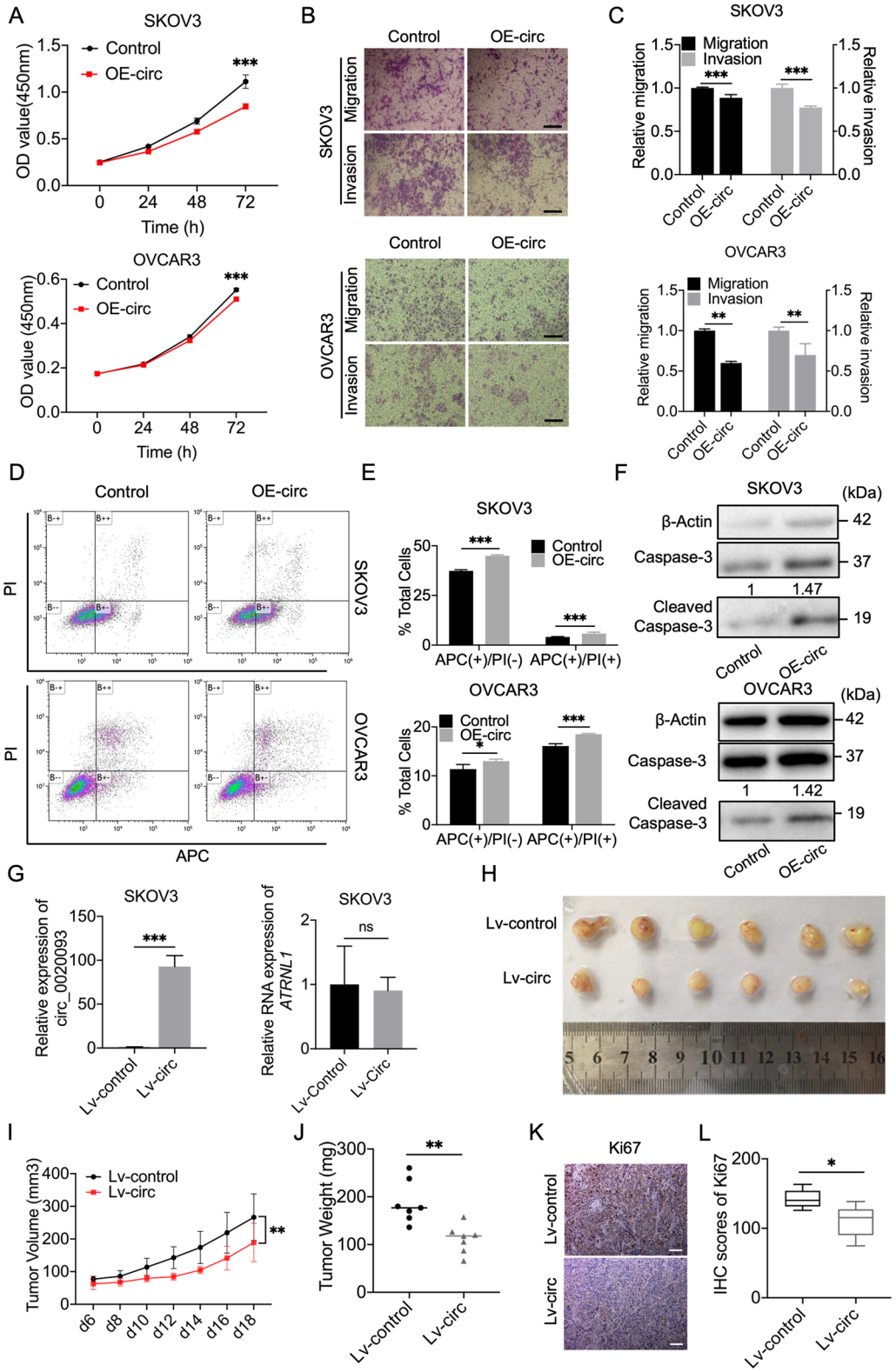

Fig. 2 (See legend on previous page.)

results suggested that *LRPPRC* may have tumor-promoting effects in OC.

hsa_circ_0020093 regulates mitochondria mRNA levels and mitochondria abundance at least partially through inhibiting LRPPRC activity in OC cells

As a multifunctional protein, LRPPRC is also involved in RNA splicing process and has the potential to regulate the biogenesis of circRNAs. However, no detectable change of hsa_circ_0020093 level was found after silencing *LRPPRC* (Online Resource 2, Supplementary Fig. 3A). Meanwhile, there was no obvious change in the mRNA and protein level of LRPPRC upon hsa_circ_0020093-overexpressing in OC cells (Online Resource 2, Supplementary Fig. 3B–C), indicating that LRPPRC and hsa_circ_0020093 didn't regulate the expression mutually.

As shown in Fig. 3G, LRPPRC was highly enriched in the cytoplasm and more than 90% of LRPPRC are colocalized with TOM20 in OC cells. A lot of studies have shown that the cytoplasm-localized LRPPRC mainly regulates energy metabolism through regulating the expression of mitochondria genes at the transcriptional and posttranscriptional levels [21–25]. We first analyzed the mRNA levels of mitochondria genes through RT-qPCR, interestingly, we observed significant downregulation of mitochondria-mRNA (MT-mRNAs) after overexpressing hsa_circ_0020093, which could be rescued by LRPPRC overexpression in SKOV3 cells (Fig. 4A). And there are fewer mitochondria in SKOV3 cells stably overexpressing hsa_circ_0020093 as compared to the control (Fig. 4B–C). These findings demonstrated that hsa_circ_0020093 decreased mitochondria mRNA levels and mitochondria abundance in OC at least partially through interacting with LRPPRC.

hsa_circ_0020093 sponges miR-107 to upregulate LATS2 expression

We also noticed that a small fraction of hsa_circ_0020093 was not colocalized with TOM20 (Fig. 3G). hsa_circ_0020093 and other cytoplasm localized circRNAs are mainly reported as miRNA sponges to prevent mRNA from being degraded by RNA-induced silencing complex (RISC) [9, 26, 27]. We also investigated the miRNA sponge potential of hsa_circ_0020093 in OC cells. Consistent with the studies before [9], RIP followed by RT-qPCR results showed that hsa_circ_0020093 could bind with argonaute-2 (AGO2), the executor of RISC [28] (Fig. 5A), indicating that hsa_circ_0020093 might regulate miRNA-mediated degradation of mRNAs. Then bioinformatic tools (TargetScan, RegRNA, StarBase) were used to predict the putative miRNAs interacted with hsa_circ_0020093 (Online Resource 1, Supplementary Table 5). The potential binding miRNAs intersected with the set of upregulated miRNAs in high-grade serous ovarian cancer samples from the GEO dataset (GSE47841) was shown in Venn diagram Fig. 5B. According to the previous studies, miR-181a-5p was associated with short PFS and OS in OC patients [29]; high expressed miR-107 played a cancer-promoting role in various tumors, including OC; while miR-378c [30, 31] and miR-422a [32, 33] inhibited cancer progression. Therefore, we chose miR-181a-5p and miR-107 to further verify the ceRNA network.

We co-transfected 293 T cells with miRNA mimics and wild-type of or the miRNA-binding-site mutant-type of linear hsa_circ_00200093 plasmid. The luciferase activity was significantly decreased in the circ-WT + miR-107 group nor other groups, suggesting that hsa_circ_0020093 could bind to miR-107 (Fig. 5D–F). Next, we used TargetScan, miRTarbase and miRDB to predict the potential mRNA regulated by miR-107 and intersected these data with our RNA sequencing results (Fig. 5G, Online Resource 1, Supplementary Tables 6 and 7), finally 19 candidate mRNAs were identified. After examining the mRNA levels of these mRNAs in GEPIA database, 6 of the 19 mRNAs were found to be downregulated in OC tissues (*BAZ2A*, *MAP3K7*, *OGT*, *PIK3R1*, *LATS2*, *DICER1*). However, *LATS2* was the only up-regulated one in hsa_circ_0020093-overexpressing cells (Fig. 5H–I), while its low level caused by miR-107 could be rescued by

(See figure on next page.)

Fig. 3 hsa_circ_0020093 directly binds to LRPPRC protein. **A** RT-qPCR analysis of hsa_circ_0020093 expression in nuclei- and cytoplasm-extracted RNA. **B** Fluorescence in situ hybridization (FISH) analysis of hsa_circ_0020093 (red) localization in SKOV3 and OVCAR3 cells. Nuclei were stained with DAPI. Scale Bar: 10 μm. **C** The silver staining results of the proteins pulled down by hsa_circ_0020093-specific probe and control probe. **D** The top 20 potential binding proteins of hsa_circ_0020093 identified by mass spectrometry analysis of the differential silver-stained bands. **E** Western blot analysis of LRPPRC following RNA pull-down confirmed the interaction between hsa_circ_0020093 and LRPPRC. **F** LRPPRC RIP assay proved the enrichment of hsa_circ_0020093 in LRPPRC-bound RNA. *P* value was calculated by two-tailed Student's t-test. **G** Combined Immunofluorescence (IF) and FISH staining were performed to detect the localization of hsa_circ_0020093 (red) and LRPPRC (green). TOM20 (purple) represents mitochondria localization. Scale Bar: 10 μm. **H** LRPPRC protein levels in OC and adjacent normal tissues from the CPTAC database are shown. **I-J** Overall survival and recurrence-free survival analysis of EOC patients with high or low expression of LRPPRC (n = 22 in each group). The significance of the differences between the survival probability was calculated by log-rank test. $^{**}P < 0.01$; $^{***}P < 0.001$

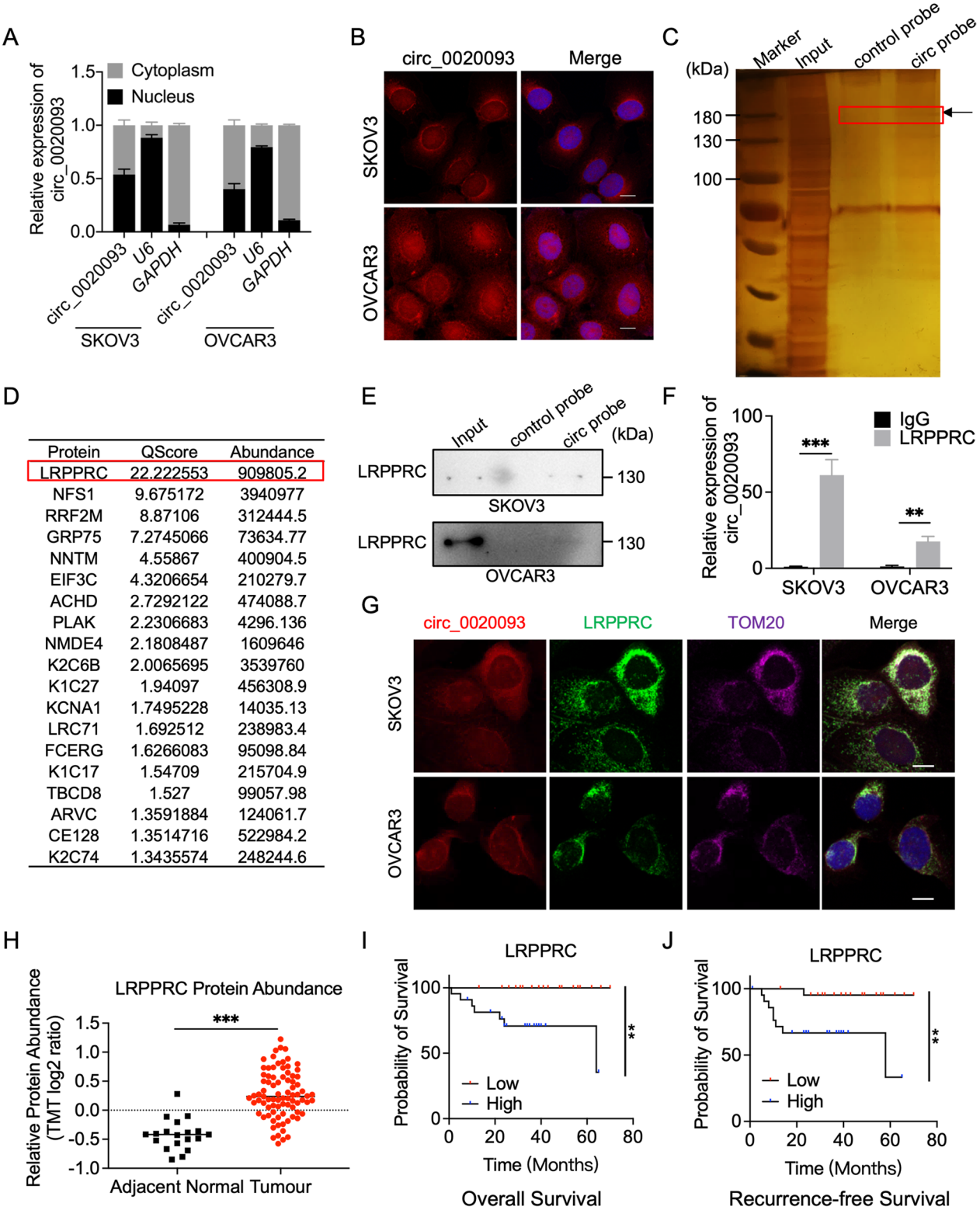

Protein	QScore	Abundance
LRPPRC	22.222553	909805.2
NFS1	9.675172	3940977
RRF2M	8.87106	312444.5
GRP75	7.2745066	73634.77
NNTM	4.55867	400904.5
EIF3C	4.3206654	210279.7
ACHD	2.7292122	474088.7
PLAK	2.2306683	4296.136
NMDE4	2.1808487	1609646
K2C6B	2.0065695	3539760
K1C27	1.94097	456308.9
KCNA1	1.7495228	14035.13
LRC71	1.692512	238983.4
FCERG	1.6266083	95098.84
K1C17	1.54709	215704.9
TBCD8	1.527	99057.98
ARVC	1.3591884	124061.7
CE128	1.3514716	522984.2
K2C74	1.3435574	248244.6

Fig. 3 (See legend on previous page.)

Table 2 Correlation between IHC score of LRPPRC and clinicopathologic factors of OC patients

Parameter		LRPPRC (Low, n = 22)	LRPPRC (High, n = 22)	*P* value
Age	≤ 50	6	8	0.517
	> 50	16	14	
FIGO Stage	I–II	17	7	**0.002****
	III–IV	5	15	
Grade	Low (G1,G2)	3	4	0.5
	High (G3)	19	18	
Lymphatic metastasis	No	18	14	0.176
	Yes	4	8	
Peritoneal implantation	No	15	7	**0.016***
	Yes	7	15	
CA125 (U/mL)	< 35	7	6	0.741
	≥ 35	15	16	

The bold numbers refer to the P value statistically significant, ** indicates that $P < 0.01$

overexpression of hsa_circ_0020093 (Fig. 5J). Together, the results demonstrated that hsa_circ_0020093 could act as miR-107 sponges to upregulate *LATS2* expression.

The interplay between hsa_circ_0020093, miR-107, LRPPRC and YAP

Apart from being the mitochondria regulator, Li et al. also found that the downregulation of LRPPRC could increase P-YAP and YAP abundance [34]. LATS2 was also known as the upstream kinase of YAP, whose upregulation is associated with the phosphorylation and inactivation of YAP [35]. The possibility of LRPPRC/LATS2 axis was first excluded as there was no detectable change of LATS2 upon LRPPRC-silencing (Online Resource 2, Supplementary Fig. 4). Consistent with Li's finding, silencing of *LRPPRC* increased both the protein level of YAP and P-YAP (Fig. 6A), while hsa_circ_0020093-overexpression only increased the protein level of P-YAP (Fig. 6B). This is possibly the results of excessively increased p-YAP by both pathways. The inactivation of YAP was confirmed by the decreased expression of YAP-targeted mRNAs *CTGF* [36], *MYC* [37], *BIRC5* [38], *MCM3* [39], and *CAV1N1* [40] after silencing *LRPPRC* or overexpressing hsa_circ_0020093 in SKOV3 cells (Fig. 6C–D). Moreover, IHC staining confirmed a higher P-YAP positive rate in xenograft tumors formed by hsa_circ_0020093-overexpressed SKOV3 cells, while YAP positive rate remained unchanged (Fig. 6E–F). The increased P-YAP level and decreased YAP-downstream mRNAs in hsa_circ_0020093-overexpressing and *LRPPRC*-silencing OC cells indicated that hsa_circ_0020093 might control YAP activity via synergistically sponging miR-107 and inhibiting LRPPRC.

Discussion

One circRNA may possess hundreds or thousands of miRNA binding sites, whether they can bind and sponge the specific miRNAs in specific tissues may be strictly regulated. Accumulating evidence has demonstrated that one single circRNA could sponge different miRNAs in the same tissues or cell lines, for example, in OC cells, CDR1as could sponge miR-135b-5p [41], miR-1299 [42], and miR-1270 [43], and circITCH could sponge miR-145 [44] or miR-106a [45]. According to recent studies, hsa_circ_0020093 could also sponge miR-378a-3p and miR-152-5p in OC cells [8, 9], miR-141-3p and miR-103a-3p in endometrial carcinoma cells [46, 47] as well as miR-338-3p, miR-181-5p, miR-23b and miR-153-3p in chondrocyte [48–51].

Due to the lack of high throughput technology for the identification and verification of all miRNAs that are sponged by the specific circRNA, our study chose miR-107 and miR-181-5p for further analysis based on the candidate miRNAs' abundance and their reported function in OC. We did not exclude other miRNAs that may be sponged by hsa_circ_0020093 in OC. Indeed, miR-107 shares the same binding sites with miR-103a-3p, providing the probability of the interaction between hsa_circ_0020093 and miR-103a-3p in OC cells. Although with limitations, our study provided experimental evidence that hsa_circ_0020093 sponged miR-107 in OC cells and expanded the miRNA pools that are sponged by hsa_circ_0020093 in OC cells.

The peri-nuclear enriched signal of the probe for hsa_circ_0020093 lets us re-think the function of hsa_circ_0020093 where we found hsa_circ_0020093 also binds and co-localizes with the mitochondria protein LRPPRC, and thus modulates the mitochondria mRNA expression and mitochondria abundance in OC cells, which is consistent with the reported LRPPRC functions [24, 25]. Our study first provides the experimental evidence that hsa_circ_0020093 also sponges the mitochondria protein LRPPRC, revealing the mechanism of action of cytoplastic localized circRNAs. Unfortunately, we haven't analyzed the change of energy metabolism after silencing of LRPPRC or overexpressing of hsa_circ_0020093, which needs to be further clarified in the future.

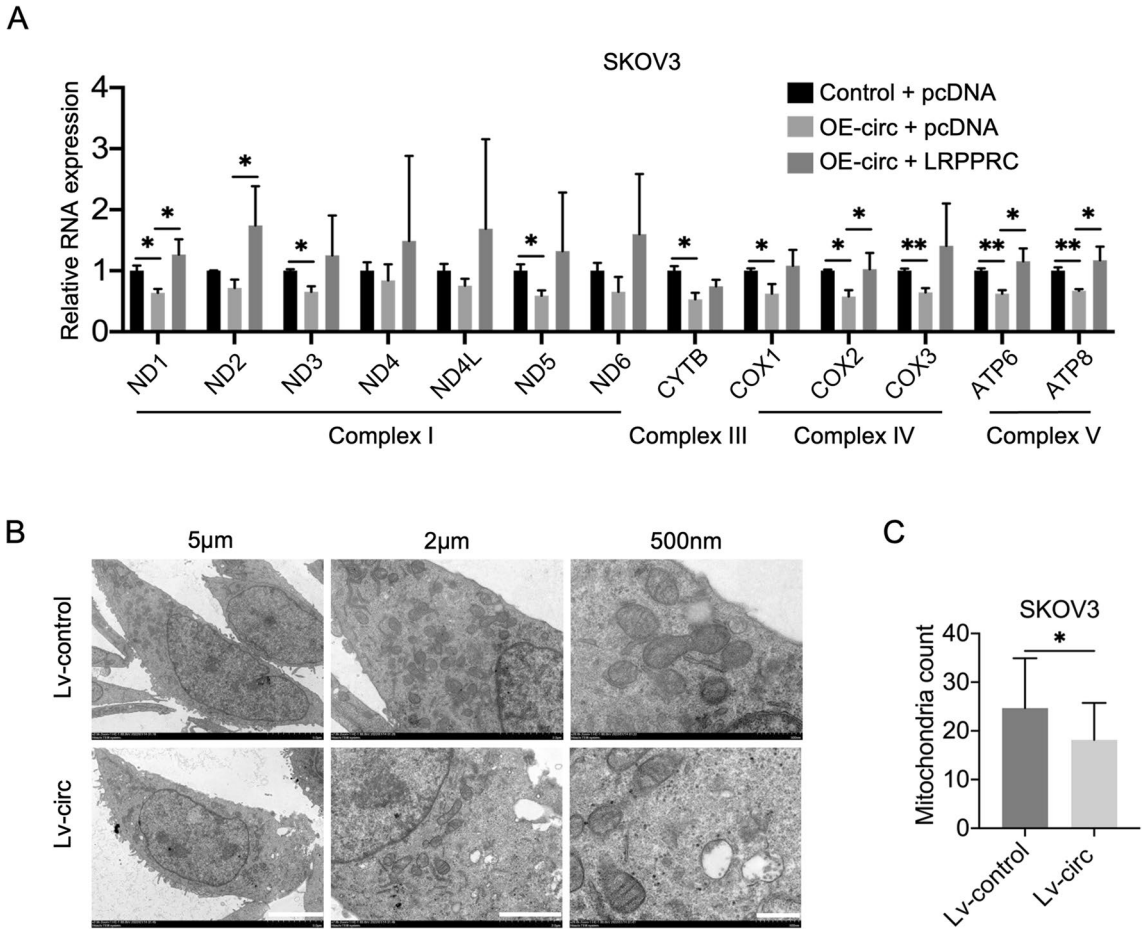

Fig. 4 hsa_circ_0020093 regulates mitochondrial mRNA expression and mitochondria abundance at least partially by inhibiting LRPPRC activity. **A** RT-qPCR analysis of the abundance of 13 mitochondrial mRNAs following co-transfection of hsa_circ_0020093-overexpressing or control and *LRPPRC*-overexpressing or pcDNA (control) plasmids. *P* value was calculated by one-way ANOVA. **B** The morphology and abundance of mitochondria were observed under transmission electron microscopy. Scale bar: 5 μm, 2 μm and 500 nm respectively. **C** The mitochondria number per cell in SKOV3 cells with stable transfection of control and hsa_circ_0020093. *P* value was calculated by two-tailed Student's t-test. $^{*}P < 0.05$; $^{**}P < 0.01$

The role of the mitochondria protein LRPPRC in OC has not yet been explored before. Our study first demonstrated that the LRPPRC protein level was negatively correlated with OC prognosis and its depletion impaired the cell viability and enhanced apoptosis of OC induced by cisplatin. Meanwhile, we also preliminarily studied the interplay between hsa_circ_0020093, miR-107/LATS2, LRPPRC and their common downstream target, YAP, providing new evidence for our understanding of the complex regulatory network within OC. However, whether their interplay is also involved in the energy metabolism of OC cells still needs to be verified.

(See figure on next page.)

Fig. 5 hsa_circ_0020093 acts as miR-107 sponge to regulate *LATS2* expression. **A** AGO2 RIP assay was executed in SKOV3 cells. **B** Venn diagram of the predicted target miRNAs of hsa_circ_0020093 identified from GSE47481, TargetScan, RegRNA and Starbase. **C** Differential expression of overlapped miRNAs across normal and high-grade serous ovarian cancer (HGSOC) samples in GSE47841. **D** Schematic illustration of hsa_circ_0020093-WT and hsa_circ_0020093-MUT luciferase reporter vectors. **E-F** The relative luciferase activities were detected in 293 T cells after co-transfection with hsa_circ_0020093-WT or hsa_circ_0020093-MUT and mimics or miRNC, respectively. **G** Venn diagram of the predicted target genes of miR-107 identified from RNA-seq data and three tools (TargetScan, miRTarbase, miRDB). **H** RT-qPCR detection of the expression of upregulated mRNAs in hsa_circ_0020093-overexpressed OC cells. **I** Western blot analysis of LATS2 protein level after hsa_circ_0020093 overexpression in OC cells. **J** Western blot analysis of LATS2 protein level after co-transfection of hsa_circ_0020093 or control and miR-107 or miRNC, respectively, in OC cells. *P* values were calculated by two-tailed Student's t test. ns, not significant; $^{*}P < 0.05$; $^{**}P < 0.01$; $^{***}P < 0.001$

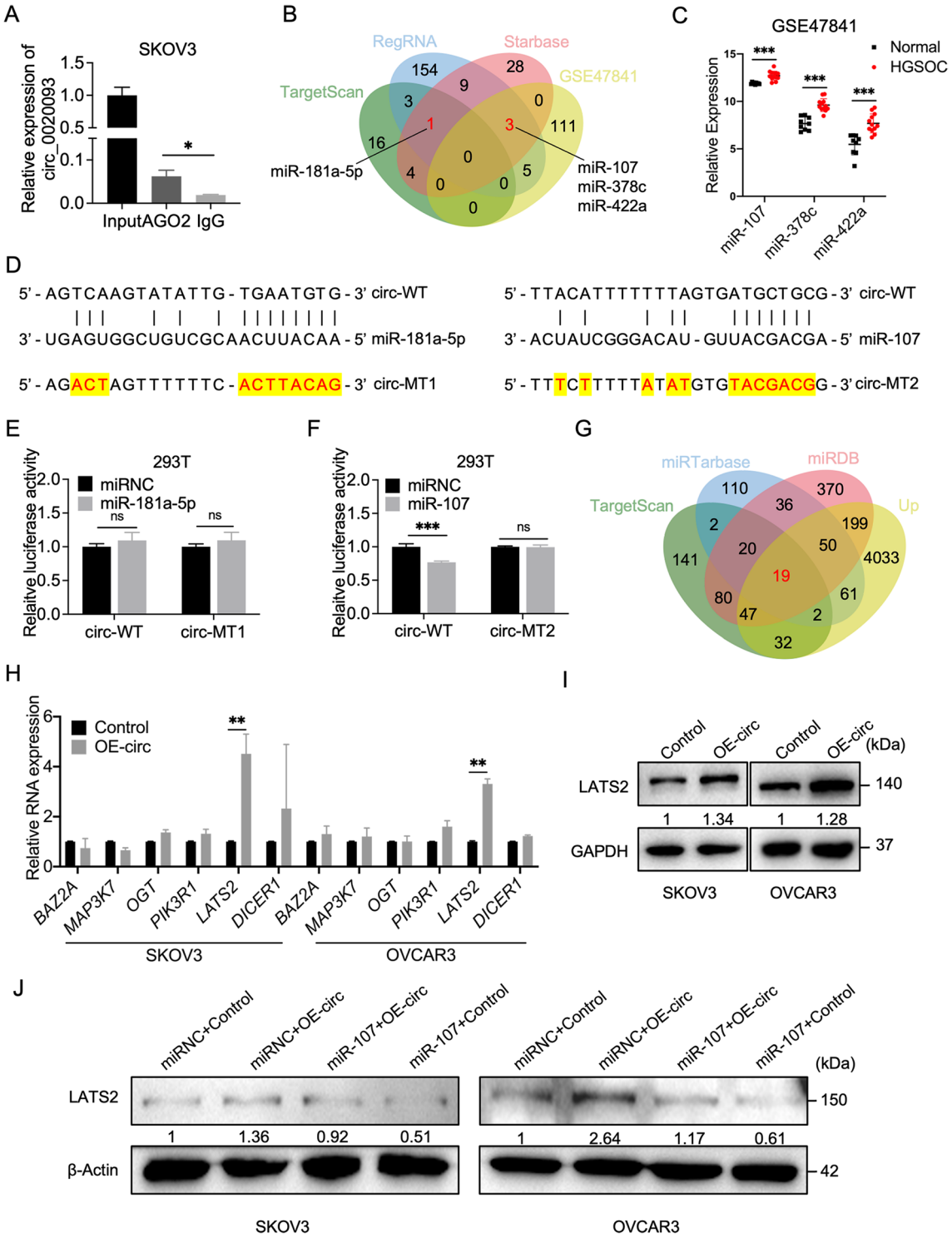

Fig. 5 (See legend on previous page.)

In summary, our data demonstrate that overexpression of hsa_circ_0020093 exerts tumor inhibitory effect by impairing OC cells proliferation, migration and invasion, enhancing cisplatin-mediated apoptosis through sponging miR-107 and LRPPRC. We also unlocked the oncogenic role of LRPPRC in OC and preliminarily analyzed the interplay between hsa_circ_0020093, miR_107 and LRPPRC in OC (Fig. 7).

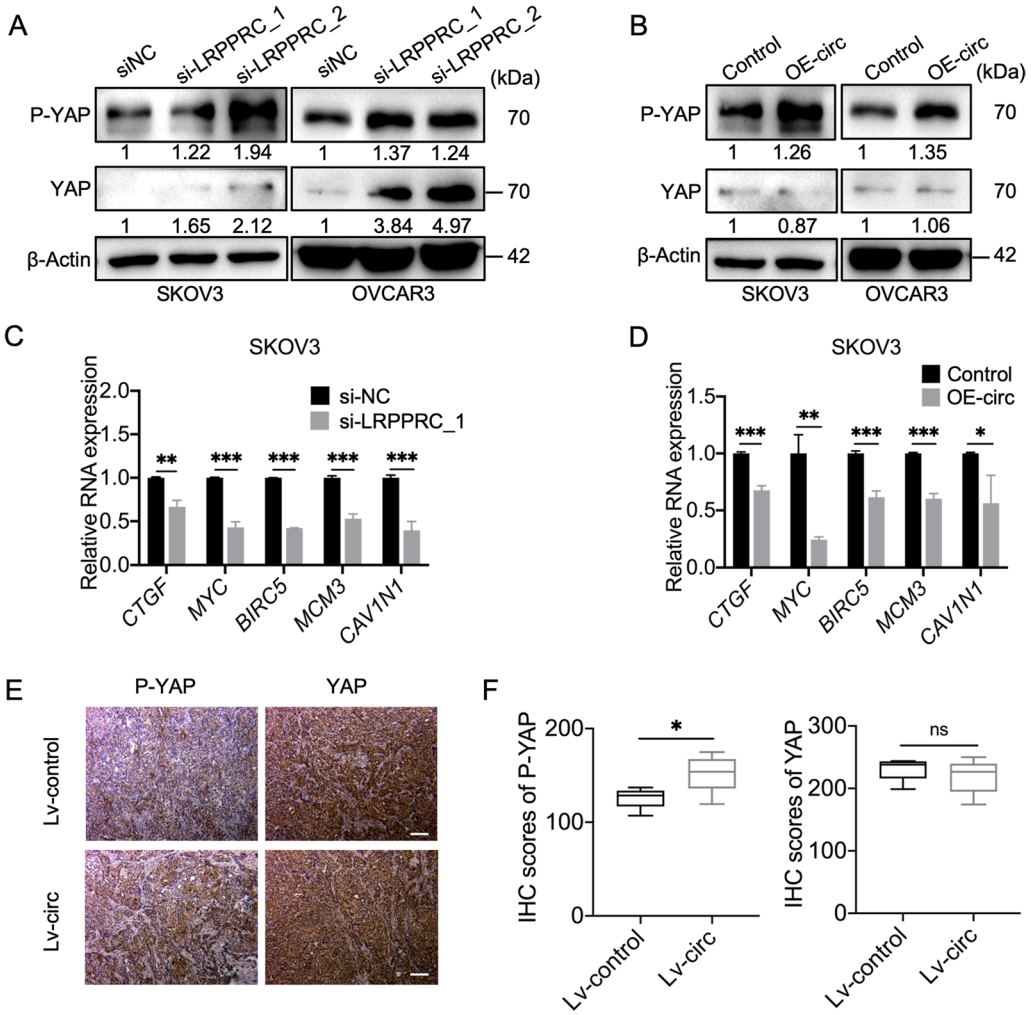

Fig. 6 Both hsa_circ_0020093 and LRPPRC regulates YAP activity. **A** Western blot analysis of P-YAP and YAP expression in LRPPRC-silencing and control OC cells. **B** Western blot analysis of P-YAP and YAP expression in hsa_circ_0020093-overexpressing and control OC cells. **C** RT-qPCR analysis of the expression of YAP-targeted mRNAs in *LRPPRC*-silencing and control SKOV3 cells. **D** RT-qPCR analysis of the expression YAP-targeted mRNAs in hsa_circ_0020093-overexpressing and control SKOV3 cells. **E** P-YAP and YAP protein level in xenograft tumors formed by control or hsa_circ_0020093 stably overexpressed SKOV3 cells were manifested by IHC staining. Scale Bar: 100 μm. **F** The IHC score of P-YAP and YAP in xenograft tumors formed by control or hsa_circ_0020093 stably overexpressed SKOV3 cells. *P* values were calculated by two-tailed Student's t-test. ns: not significant; $^{*}P < 0.05$; $^{**}P < 0.01$; $^{***}P < 0.001$

Schematic illustrating the main finding of this study: hsa_circ_0020093 potentially controls YAP activity via synergistically sponging miR-107 as well as LRPPRC and regulates mitochondria-mediated signaling pathway by inhibiting LRPPRC.

Conclusions

Taken together, we identified a tumor suppressive circRNA, hsa_circ_0020093, whose expression is negatively correlated with the FIGO stage, abdominal implantation, and CA125 level of OC patients. We found that hsa_circ_0020093 could simultaneously sponge the

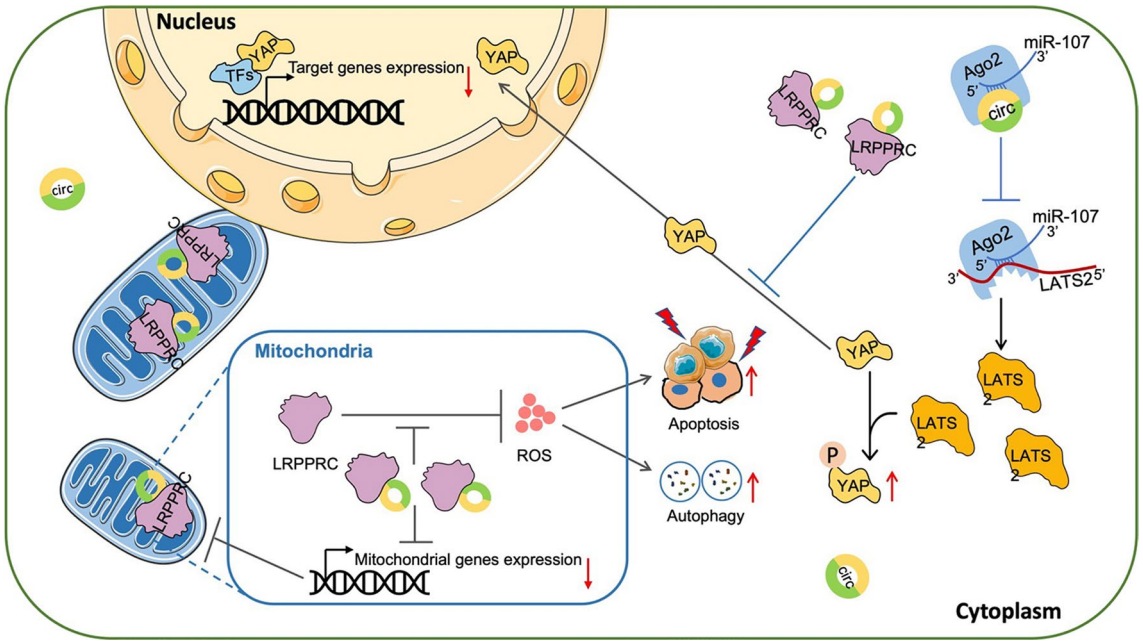

Fig. 7 The schematic diagram shows the mechanism of hsa_circ_0020093 regulating OC progression

mitochondria protein LRPPRC and miR_107 to regulate their downstream signaling pathways. Indicating that hsa_circ_0020093 can act as a promising prognostic biomarker and new therapeutic target for OC.

Abbreviations

OC	Ovarian cancer
circRNAs	Circular RNAs
CCK-8	Cell Counting Kit-8
RT-qPCR	Quantitative Reverse Transcription Polymerase Chain Reaction
RIPA	Radioimmunoprecipitation assay
SSC	Saline-sodium Citrate
RIP	RNA Immunoprecipitation
FISH	Fluorescence in situ Hybridization
IF	Immunofluorescence
IHC	Immunohistochemistry
mtROS	Mitochondrial reactive oxygen species
RISC	RNA-induced silencing complex

Supplementary Information

The online version contains supplementary material available at https://doi.org/10.1186/s13062-024-00520-y.

Additional file 1.

Additional file 2.

Acknowledgements
None.

Author contributions
X.J. and J.X. and L.G. conceptualized, supervised, administered the whole project, reviewed the manuscript, and acquired funding; Y.S. and X.C. designed, analyzed, and interpreted the experiments and wrote the original manuscript. YQ.S. and C.D. improved formal analysis, visualization, and data curation. F.T. provides data collection and validation, as well as funding. All authors reviewed the manuscript.

Funding
This work was supported by National Natural Science Foundation of China under grant #81902651; Jiangsu Provincial Key Research and Development Program under grant #BE2020753; "333 Project" of Jiangsu Province under grant J. X. and X. M. J.; Jiangsu Maternal and Child Health Research Project under grant #F202106; and Nanjing Medical Science and Technique Development Foundation under grant #ZKX21051; and Jiangsu Province Capability Improvement Project through Science, Technology and Education Jiangsu Provincial Medical Key Discipline under grant #ZDXK202211.

Data availability
All the data were available in supplementary information online or from the corresponding author on reasonable request.

Declarations

Ethics approval and consent to participate
The study was approved by the Ethics Committee of Women's Hospital of Nanjing Medical University (approval number: 2022KY-176) and all participants signed informed consent forms. All experiments of this study were carried out in accordance with the approved guidelines and regulations. Animal experiments were conducted in accordance with ARRIVE guidelines and the protocols approved by Nanjing Medical University (approval number: IACUC-2208015). Informed consent was obtained from all individual participants included in the study.

Competing interests
The authors declares that no competing interests.

Received: 17 May 2024 Accepted: 8 August 2024
Published online: 21 August 2024

References

1. Sung H, Ferlay J, Siegel RL, et al. Global cancer statistics 2020: GLOBOCAN estimates of incidence and mortality Worldwide for 36 cancers in 185 Countries. CA Cancer J Clin. 2021;71(3):209–49.

2. Siegel RL, Miller KD, Wagle NS, Jemal A. Cancer statistics. CA Cancer J Clin. 2023;73(1):17–48.
3. Menon U, Gentry-Maharaj A, Burnell M, et al. Ovarian cancer population screening and mortality after long-term foll ow-up in the UK Collaborative Trial of Ovarian Cancer Screening (UKCTO CS): a randomised controlled trial. Lancet (London, England). 2021;397(10290):2182–93.
4. Goodall GJ, Wickramasinghe VO. RNA in cancer. Nat Rev Cancer. 2021;21(1):22–36.
5. Kristensen LS, Jakobsen T, Hager H, Kjems J. The emerging roles of circRNAs in cancer and oncology. Nat Rev Clin Oncol. 2022;19(3):188–206.
6. He AT, Liu J, Li F, Yang BB. Targeting circular RNAs as a therapeutic approach: current strategies and challenges. Signal Transduct Target Ther. 2021;6(1):185.
7. Meganck RM, Borchardt EK, Castellanos Rivera RM, et al. Tissue-dependent expression and translation of circular RNAs with recombinant AAV vectors in vivo. Mol Ther Nucleic Acids. 2018;13:89–98.
8. Teng F, Xu J, Zhang M, et al. Comprehensive circular RNA expression profiles and the tumor-suppressive function of circHIPK3 in ovarian cancer. Int J Biochem Cell Biol. 2019;112:8–17.
9. Wang J, Li Y, Zhou JH, et al. CircATRNL1 activates Smad4 signaling to inhibit angiogenesis and ovarian cancer metastasis via miR-378. Mol Oncol. 2021;15(4):1217–33.
10. Lyu M, Li X, Shen Y, et al. CircATRNL1 and circZNF608 inhibit ovarian cancer by Sequestering miR-152-5p and encoding protein. Front Genet. 2022;13: 784089.
11. Zhao W, Cui Y, Liu L, et al. Splicing factor derived circular RNA circUHRF1 accelerates oral squamous cell carcinoma tumorigenesis via feedback loop. Cell Death Differ. 2020;27(3):919–33.
12. Pan X, Geng Z, Li J, et al. Peptide PDHPS1 inhibits ovarian cancer growth through disrupting YAP signaling. Mol Cancer Ther. 2022;21(7):1160–70.
13. Varghese F, Bukhari AB, Malhotra R, De A. IHC Profiler: an open source plugin for the quantitative evaluation and automated scoring of immunohistochemistry images of human tissue samples. PLoS ONE. 2014;9(5): e96801.
14. Huang X, He M, Huang S, et al. Circular RNA circERBB2 promotes gallbladder cancer progression by regulating PA2G4-dependent rDNA transcription. Mol Cancer. 2019;18(1):166.
15. Wang D, Qian X, Du Y-CN, et al. Abstract 3912: cProSite: A web based interactive platform for on-line proteomics and phosphoproteomics data analysis. Cancer Res. 2022;82(12):3912–3912.
16. Kristensen LS, Andersen MS, Stagsted LVW, et al. The biogenesis, biology and characterization of circular RNAs. Nat Rev Genet. 2019;20(11):675–91.
17. Cui J, Wang L, Ren X, et al. LRPPRC: a multifunctional protein involved in energy metabolism and human disease. Front Physiol. 2019;10:595.
18. Jiang X, Li X, Huang H, et al. Elevated levels of mitochondrion-associated autophagy inhibitor LRPPRC are associated with poor prognosis in patients with prostate cancer. Cancer. 2014;120(8):1228–36.
19. Wang L, Luo J, Li Y, et al. Mitochondrial-associated protein LRPPRC is related with poor prognosis potentially and exerts as an oncogene via maintaining mitochondrial function in pancreatic cancer. Front Genet. 2021;12: 817672.
20. Li X, Lv L, Zheng J, et al. The significance of LRPPRC overexpression in gastric cancer. Med Oncol. 2014;31(2):818.
21. Mili S, Shu HJ, Zhao Y, PiñOl-Roma SN. Distinct RNP complexes of shuttling hnRNP proteins with Pre-mRNA and mRNA: candidate intermediates in formation and export of mRNA. Mol Cell Biol. 2001;21(21):7307–19.
22. Siira SJ, Spåhr H, Shearwood AJ, et al. LRPPRC-mediated folding of the mitochondrial transcriptome. Nat Commun. 2017;8(1):1532.
23. Ruzzenente B, Metodiev MD, Wredenberg A, et al. LRPPRC is necessary for polyadenylation and coordination of translation of mitochondrial mRNAs. Embo j. 2012;31(2):443–56.
24. Sasarman F, Brunel-Guitton C, Antonicka H, et al. LRPPRC and SLIRP interact in a ribonucleoprotein complex that regulates posttranscriptional gene expression in mitochondria. Mol Biol Cell. 2010;21(8):1315–23.
25. Cuillerier A, Honarmand S, Cadete VJJ, et al. Loss of hepatic LRPPRC alters mitochondrial bioenergetics, regulation of permeability transition and trans-membrane ROS diffusion. Hum Mol Genet. 2017;26(16):3186–201.
26. Salmena L, Poliseno L, Tay Y, et al. A ceRNA hypothesis: the Rosetta Stone of a hidden RNA language? Cell. 2011;146(3):353–8.
27. Thomson DW, Dinger ME. Endogenous microRNA sponges: evidence and controversy. Nat Rev Genet. 2016;17(5):272–83.
28. Li X, Wang X, Cheng Z, Zhu Q. AGO2 and its partners: a silencing complex, a chromatin modulator, and new features. Crit Rev Biochem Mol Biol. 2020;55(1):33–53.
29. Petrillo M, Zannoni GF, Beltrame L, et al. Identification of high-grade serous ovarian cancer miRNA species associated with survival and drug response in patients receiving neoadjuvant chemotherapy: a retrospective longitudinal analysis using matched tumor biopsies. Ann Oncol. 2016;27(4):625–34.
30. Li J, Xiang Q, Wang M, et al. All-trans retinoic acid enhances chemosensitivity to 5-FU by targeting miR-378c/E2F7 axis in colorectal cancer. J Oncol. 2021;2021:5338934.
31. Yu Q, Zheng B, Ji X, et al. miR-378c suppresses Wilms tumor development via negatively regulating CAMKK2. Acta Biochim Biophys Sin (Shanghai). 2021;53(6):739–47.
32. Wang L, Chen J, Lu C. Circular RNA Foxo3 enhances progression of ovarian carcinoma cells. Aging (Albany NY). 2021;13(18):22432–43.
33. He Z, Li Z, Zhang X, et al. MiR-422a regulates cellular metabolism and malignancy by targeting pyruvate dehydrogenase kinase 2 in gastric cancer. Cell Death Dis. 2018;9(5):505.
34. Li W, Dai Y, Shi B, et al. LRPPRC sustains Yap-P27-mediated cell ploidy and P62-HDAC6-mediated autophagy maturation and suppresses genome instability and hepatocellular carcinomas. Oncogene. 2020;39(19):3879–92.
35. Ma S, Meng Z, Chen R, Guan KL. The hippo pathway: biology and pathophysiology. Annu Rev Biochem. 2019;88:577–604.
36. Zhao B, Ye X, Yu J, et al. TEAD mediates YAP-dependent gene induction and growth control. Genes Dev. 2008;22(14):1962–71.
37. Wang H, Zhang S, Zhang Y, et al. TAZ is indispensable for c-MYC-induced hepatocarcinogenesis. J Hepatol. 2022;76(1):123–34.
38. Rosenbluh J, Nijhawan D, Cox AG, et al. β-Catenin-driven cancers require a YAP1 transcriptional complex for survival and tumorigenesis. Cell. 2012;151(7):1457–73.
39. Tóth M, Wehling L, Thiess L, et al. Co-expression of YAP and TAZ associates with chromosomal instability in human cholangiocarcinoma. BMC Cancer. 2021;21(1):1079.
40. Rausch V, Bostrom JR, Park J, et al. The hippo pathway regulates caveolae expression and mediates flow response via caveolae. Curr Biol. 2019;29(2):242-255.e246.
41. Chen H, Mao M, Jiang J, et al. Circular RNA CDR1as acts as a sponge of miR-135b-5p to suppress ovarian cancer progression. Onco Targets Ther. 2019;12:3869–79.
42. Wu H, Zhao X, Wang J, et al. Circular RNA CDR1as alleviates cisplatin-based chemoresistance by suppressing MiR-1299 in ovarian cancer. Front Genet. 2021;12: 815448.
43. Zhao Z, Ji M, Wang Q, et al. Circular RNA Cdr1as upregulates SCAI to suppress cisplatin resistance in ovarian cancer via miR-1270 suppression. Mol Ther Nucleic Acids. 2019;18:24–33.
44. Hu J, Wang L, Chen J, et al. The circular RNA circ-ITCH suppresses ovarian carcinoma progression through targeting miR-145/RASA1 signaling. Biochem Biophys Res Commun. 2018;505(1):222–8.
45. Lin C, Xu X, Yang Q, et al. Circular RNA ITCH suppresses proliferation, invasion, and glycolysis of ovarian cancer cells by up-regulating CDH1 via sponging miR-106a. Cancer Cell Int. 2020;20:336.
46. Chen X, Liu M. CircATRNL1 increases acid-sensing ion channel 1 to advance epithelial-mesenchymal transition in endometriosis by binding to microRNA-103a-3p. Reprod Biol. 2022;22(2): 100643.
47. Wang D, Luo Y, Wang G, Yang Q. CircATRNL1 promotes epithelial-mesenchymal transition in endometriosis by upregulating Yes-associated protein 1 in vitro. Cell Death Dis. 2020;11(7):594.
48. Zheng J, Lin Y, Tang F, et al. Promotive role of CircATRNL1 on chondrogenic differentiation of BMSCs mediated by miR-338-3p. Arch Med Res. 2021;52(5):514–22.

49. Zhu J, Guo Y. Circ_0020093 overexpression alleviates interleukin-1 beta-induced inflammation, apoptosis and extracellular matrix degradation in human chondrocytes by targeting the miR-181a-5p/ERG Pathway. Immunol Invest. 2022;51(6):1660–77.
50. Feng M, Jing L, Cheng J, et al. Circ_0020093 ameliorates IL-1beta-induced apoptosis and extracellular matrix degradation of human chondrocytes by upregulating SPRY1 via targeting miR-23b. Mol Cell Biochem. 2021;476(10):3623–33.
51. Wang KF, Shi ZW, Dong DM. CircATRNL1 protects against osteoarthritis by targeting miR-153-3p and KLF5. Int Immunopharmacol. 2021;96: 107704.

Publisher's Note